Article

Analysis of Measurements of Direct Normal and Global Solar Radiation for Maceió, Alagoas State, Northeastern Brazil

José Marcelo Lopes Júnior[1], José Leonaldo de Souza[1] (iD), Ricardo Araujo Ferreira Junior[1],
Cícero Manoel dos Santos[2], Gustavo Bastos Lyra[3], Chigueru Tiba[4],
Rosiberto Salustiano da Silva Júnior[1]

[1]*Setor de Agrometeorologia, Universidade Federal de Alagoas, Maceió, AL, Brasil.*
[2]*Faculdade de Agronomia, Universidade Federal do Pará, Altamira, PA, Brasil.*
[3]*Departamento de Ciências Ambientais, Universidade Federal Rural do Rio de Janeiro,
Seropédica, RJ, Brasil.*
[4]*Departamento de Energia Nuclear, Universidade Federal de Pernambuco, Recife, PE, Brasil.*

Abstract

Studying solar radiation is essential for human knowledge, since it is present in practically all its activities. Thus, the aim of this work was to analyze the climatic and seasonal variation of direct normal and global solar radiation in the region of Maceió, Alagoas State, Northeastern Brazil with sky conditions characterized by clearness index (K_t). The K_t was determined by the ratio between global solar irradiance and solar irradiance at the top of the atmosphere. The highest occurrences of daily direct normal solar irradiance under conditions of $K_t \geq 0.6$ were recorded between 400 W m^{-2} and 700 W m^{-2} for all seasons. Under conditions of $0.4 \leq K_t < 0.6$, the daily direct normal solar irradiance occurred between 200 W m^{-2} and 500 W m^{-2} and for conditions of $K_t < 0.4$, its maximum value was 200 W m^{-2}. It was observed that the levels of solar incidence in the study region depend on cloud cover conditions, with little influence of seasonality.

Keywords solar irradiance, climatic and seasonal analysis, sky conditions.

Análise das Medidas de Radiação Solar Direta Normal e Global para Maceió, Estado de Alagoas, Nordeste do Brasil

Resumo

Estudar a radiação solar é essencial para o conhecimento humano, visto que ela está presente em praticamente todas suas atividades. Assim, o objetivo desse trabalho é analisar a variação climática e sazonal da radiação solar direta normal e global na região de Maceió, estado de Alagoas, Nordeste do Brasil com condições do céu caracterizada pelo índice de claridade (K_t). O K_t foi determinado pela razão entre irradiância solar global e irradiância solar no topo da atmosfera. As maiores ocorrências de irradiância solar direta normal diária em condições de $K_t \geq 0,6$ foram registradas entre 400 W m^{-2} e 700 W m^{-2} em todas as estações do ano. Sob condições de $0,4 \leq K_t < 0,6$, a irradiância solar direta normal diária ocorreu entre 200 W m^{-2} e 500 W m^{-2} e para condições de $K_t < 0,4$, seu valor máximo foi de 200 W m^{-2}. Observou-se que os níveis de incidência solar na região de estudo dependem das condições de cobertura de nuvens, com pouca influência da sazonalidade.

Palavras-chave: irradiância solar, análise climática e sazonal, condição do céu.

1. Introduction

The radiation emitted by the Sun that arrives at Earth (top of the atmosphere and terrestrial surface) is the main source of energy that influences practically all human activities (Liou, 2002; Muneer, 2004; Santos *et al.*, 2014). The knowledge of the global solar irradiance (I_G) which is measured on a horizontal surface, direct normal solar irradiance (I_D) and diffuse solar irradiance (I_d) has great importance in several scientific and technological areas,

e.g. meteorology, climatology, energy generation, agrometeorology, and others (Vick *et al.*, 2012; Tabari and Talaee, 2014; Evseev and Kudish, 2015; Ferreira Junior *et al.*, 2015; Santos *et al.*, 2016).

Thus, solar radiation studies require reliable and readily available data series for applications at the site of interest. The instrumentation to obtain I_G and I_D time series is given by the installation of a network of solar monitoring stations with radiometers and data acquisition system. The amount and spectral distribution of I_G and I_D depend on astronomical, atmospheric and local parameters such as: solar zenith angle, aerosol concentration and properties, amount of ozone, clouds, altitude of the site and surface albedo (Kaskaoutis and Kambezidis, 2009). I_D is very sensitive to the optical depth of the aerosol and exhibits high frequency variation to the dynamic effects of clouds, showing greater spatial and temporal variability than I_G, making it difficult to characterize daily and seasonal variability of solar radiation and its components (Kotti *et al.*, 2014).

The climatic characterization of the solar radiation requires a series of long-term measurements. However, the availability of solar databases, especially long time and continuous I_D is scarce. With the availability of measurements, different researchers studied the climatic characteristics of solar irradiance, especially the work of Liu and Jordan (1960). In Beer Sheva - Israel, Evseev and Kudish (2015) analyzed solar irradiance from 1985 to 2013 and observed that the site has high frequency of clear sky days. In Seville - Spain, Moreno-Tejera *et al.* (2016) showed an analysis of solar irradiance variation, applying a statistical characterization in different time partitions.

Despite the importance and interest of the scientific and governmental community, the knowledge of solar irradiance components on the surface is still in its beginning in the Brazilian territory, mainly because it is a country of great territorial extent. In Brazil, there are few solarimetric stations that simultaneously perform high quality measurements of I_G and I_D components. Studies analyzing databases of solar components are not so often found in specialized literature; however global solar radiation for several sites in Northeastern Brazil (NEB) has been evaluated (Tiba, 2001). The seasonal variations of the diurnal evolution of solar irradiance components based on measurements collected on the surface of the city of São Paulo - Brazil (Oliveira *et al.*, 2002). The global solar irradiation was evaluated in Maceió (NEB) (Souza *et al.*, 2005), showing a lower monthly average daily value in July and higher in November, with dry season (October-February) average hourly values 12.26% higher than values in the rainy season (April-August). Analyzes and comparisons of solar components were made for the city of São Paulo and rural area of Botucatu-SP (Codato *et al.*, 2008), in which, although located in similar latitude and altitude, the seasonal evolution of the daily values indicates that São Paulo receives, during the days of open sky, 7.8% less in August and 5.1% less in June than Botucatu. An observational characterization of the diurnal and seasonal variation of the solar irradiance components for Rio de Janeiro has been Marques Filho *et al.* (2016).

The research site is located in the metropolitan region of Maceió, with sugarcane cultivation in the vicinity, bathed by the Atlantic Ocean and large lagoons; thus, the local atmosphere is polluted by particulates originating from industries, burning and local fires, and elevation of the water vapor concentration that attenuates I_G and, mainly, I_D. These very small solid or liquid particles, called aerosols, are determinants of the spread of I_D. On the other hand, water vapor acts in the earth's atmosphere as an I_D absorber. The combined action of aerosol concentration and water vapor content significantly affects the magnitude and variability of I_D, influencing the transparency level of the atmosphere. The importance of solar radiation characterization for the region where there is a growing demand for solarimetric information for solar energy, fundamental for establishing public policies in the area of renewable energy is also highlighted. Thus, this paper presents a climatic and seasonal analysis of the effects of sky cover on I_G and I_D values in the metropolitan region of Maceió between years of 2011 and 2014.

2. Material and Methods

2.1. Study area

The measurements used in this study were obtained from the solarimetric station located at the Federal University of Alagoas (9°33' S; 35°46' W and 100 m a.s.l.), in Maceió, capital of the State of Alagoas, located in eastern NEB (Fig. 1). The microregion of Maceió is located on the coast, with variation of altitude between (0 and 20) m in the lower region (coastal plain), between (20 and 180) m on the slopes and coastal boards, reaching 300 m at the northern end of the municipality (Fig. 1). This variation can cause changes in air temperature and winds. The solarimetric station is installed at 15 km from the Atlantic Ocean, with herbaceous vegetation and Atlantic Rainforest and hot and humid climate.

Alagoas is subdivided into three geographic mesoregions (Coastal/Humid Zones, Hinterland and Interior) with different types of climate and further details are described in Santos *et al.* (2014), Santos *et al.* (2016) and Barros *et al.* (2012). The microregion of Maceió is part of mesoregions of Coastal/Humid Zones. This mesoregion have hot and humid climate, with annual rainfall varying from 600 to 3000 mm, the rainy season is concentrated between autumn and winter (from May to August), with 55.2% of the annual rainfall and the dry period occurs between spring and summer (November to February) with only 12.5% of the total rainfall (Lima, 1991; Souza and
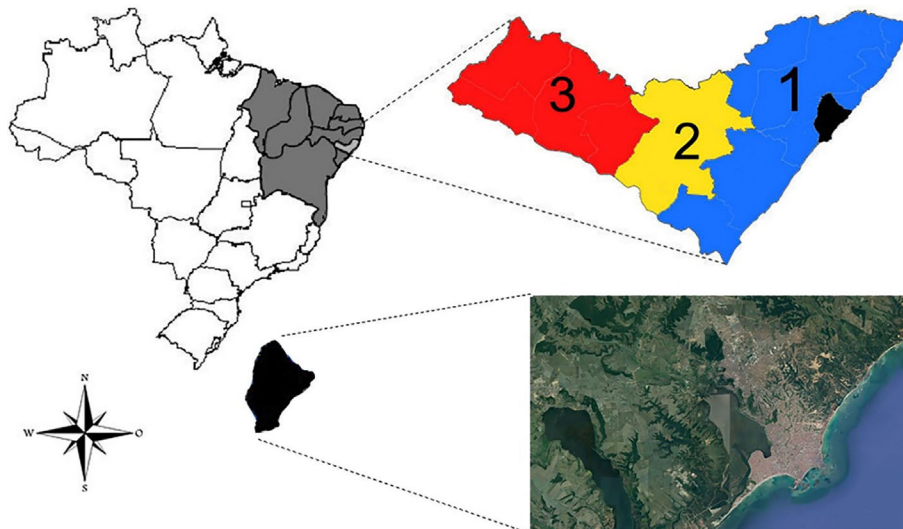
Figure 1 - Geographic location of northeastern Brazil (in dark gray), from the State of Alagoas with its mesoregions, Coastal/Humid Zones (1), Hinterland (2) and Interior (3) and municipality of Maceió (highlighted). Source: Google Maps, 2017.

Lima, 1995; Molion and Bernardo, 2002). The rainfall regime of the State of Alagoas is associated with several meteorological systems common to much NEB. Among the main systems, the coastal instability lines, seasonal variation of trade winds, position and intensity of the Intertropical Convergence Zone (ITCZ), Upper-Level Cyclonic Vortexes (ULCV), Eastern Waves (EW), are highlighted as the main ones (Souza *et al.*, 2004; Lyra *et al.*, 2014). In general, Alagoas has rainy season between May and July, when there is the maximum convergence of trade winds with the terrestrial breeze, which should be stronger during the autumn and winter seasons when the temperature contrast between land and sea is higher (Kousky, 1980), and a dry season between November and

January, a period in which a shift in the direction of trade winds takes place, which impairs the formation of clouds in the region.

2.2. Obtaining data

In this study measurements of global solar irradiance (I_G) and direct normal solar irradiance (I_D) were obtained from 2011 to 2014. Due to technical/operational problems, the I_D database used is not continuous over the measurement period. The lack of electricity and non-linearization of the sensor with the solar disk are some factors responsible for significantly reducing the database. The I_G component was measured with a piranometer model CM5 Kipp & Zonen (Delft, The Netherlands) (Fig. 2). The I_D

Figure 2 - Solarimetric station: Kipp & Zonen CM5 pyranometer and pyrheliometer assembled on the Eppley solar tracker.

component was measured by sNIP model secondary standard pyrheliometer assembled on an automatic solar tracker (Fig. 2) manufactured by Eppley. All sensors used followed the maintenance and calibration procedure according to manufacturer's recommendations (periodic calibration). Periodic checks throughout the measurements were made to ensure that the radiometer domes were clean, obtaining accurate and reliable measurements.

The radiometers used were connected to a Micrologger 21XL (Campbell Scientific Inc), with frequency of 1 Hz and programmed to take readings every 10 s and store the average every 10 min. Hourly and daily data are calculated from the average values of 10 min. The collected I_G and I_D data were integrated to produce global solar irradiation (H_G) and direct normal solar irradiation (H_D) on hourly ($H_G{}^h$ and $H_D{}^h$) and daily ($H_G{}^d$ and $H_D{}^d$) basis, respectively. A quality control process is essential before using any database of the place of interest. The quality of individual measures was verified according to recommendations of the World Meteorological Organization (WMO, 2008).

2.3. Statistical and climatic analysis of measurements

The measures of I_G (H_G) and I_D (H_D) in the hourly and daily time partitions were analyzed considering seasonality and local cloud cover. For statistical and climatic analysis of measurements, solar irradiance components were separated into periods and characterized in the different seasons of the year according to the region climatology, which is strongly dependent on the seasonality of precipitation and air temperature (Souza *et al*., 2004). In the Maceió region, the rainy season begins in April and ends in August, while the dry season begins in October and extends through February. Based on this seasonality and for further study, the climatic periods were separated into four: 1 - the dry (less rainy) period was separated into Dry Season (DS) (November to February); 2 - the transition period between dry and rainy season (March and April) was separated and defined as Pre-Rainy Season (PRS); 3 - the rainy season (May to August), will be called here as the Rainy Season (RS); 4 - the transition period between the rainy and dry season (September and October) was denominated as Pre-Dry Season (PDS).

The cloud cover was characterized from clearness index (K_t) values in the hourly ($K_t{}^h$) and daily ($K_t{}^d$) partitions, determined by the $K_t = I_G/I_0$ ratio. Thus, based on Iqbal (1983), some adaptations were made regarding K_t intervals to the atmosphere of Maceió, when ($K_t \geq 0.60$), the conditions are of Clear Sky (CS); when ($0.40 \leq K_t < 0.60$) characterizes Partially Cloudy Sky (PCS) condition and for ($K_t < 0.40$) it characterizes Overcast Sky (OS). For the representation of irradiance curves (irradiations) and estimates, days representing the different cloud cover conditions in each of the stations were randomly chosen. The I_G and I_D variations were elaborated with average mea-

sures of 10 min, and hourly curves of $H_G{}^h$ and $H_D{}^h$ were plotted from the integration of the irradiance curves for each hour. Irradiance and irradiation analyses were performed between the interval between 06:00 am and 05:00 pm, comprising practically the entire daytime period of solar incidence.

The average value of solar irradiance (global and direct) were separated into three different cloud cover conditions and four-time intervals. The average hourly of global solar irradiance ($\bar{I}_G{}^h$) with the respective standard deviations ($\delta I_G{}^h$) and the average hourly of direct normal solar irradiance ($\bar{I}_D{}^h$) with the respective standard deviations ($\delta I_D{}^h$) were calculated at each time interval. Histograms of direct normal daily solar irradiance ($I_D{}^d$) frequencies of each season of the year under study and under different cloud cover conditions were performed with the purpose of analyzing seasonal tendencies.

2.4. Calculation of solar irradiance at the top of the atmosphere

The solar irradiance at the top of the atmosphere (I_0) was calculated by Eq. (1):

$$I_0 = I_{SC} E_0 cos\theta_Z \tag{1}$$

in which I_{SC} is the solar constant (1367 W m^{-2}), E_0 is the correction factor of the eccentricity of the, further details are described in Souza *et al*. (2005) and Iqbal (1983). I_0 data were integrated to obtain the solar irradiation values at the top of the atmosphere (H_0), hourly ($H_0{}^h$) and daily ($H_0{}^d$).

3. Results and Discussion

3.1. Climate and Weather system

The climate of Maceió is "As" type, characterized as rainy tropical, with rain in the winter and autumn and dry in the summer (Köppen classification). The air temperature is high (> 20.0 °C), with monthly thermal amplitude equal to 2.9 °C, average air temperature of 23.9 °C in the coldest month (July) and 26.6 °C in the hottest (March), the average is 25.4°C (Fig. 3a). In spring and summer, it is common to have days with maximum air temperature above 30.0 °C, whereas in autumn and winter, daily air temperatures rarely reduce values below 20.0 °C. The relative air humidity presents low annual fluctuation, with monthly average values greater than 75% (Fig. 3a), which is due to its proximity to the Atlantic Ocean. Rainfall in the wettest month is 341.9 mm (June) and in the least rainy month 30.2 mm (December); summer precipitation is approximately 293.4 mm (Fig. 3b). Spring is the season with the lowest precipitation (168.8 mm).

From November to March, precipitation is usually attributed to the convergence between the land breeze and
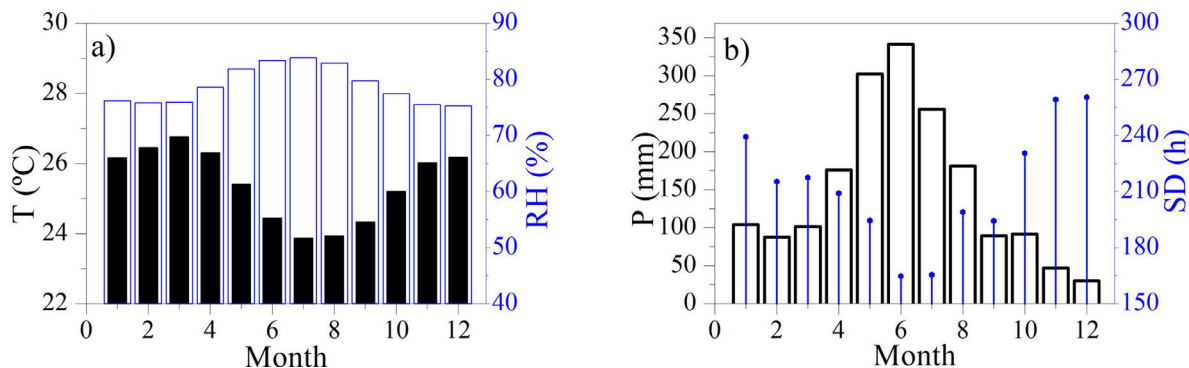
Figura 3 - Monthly average variation: a) Air temperature (T, °C) and Relative humidity (RH,%); b) Precipitation (P, mm) and sunshine duration (SD, hours). Data from 1995 to 2014 obtained from the National Institute of Meteorology (INMET).

the southeastern trade winds; however, in this time of year, this does not occur often, since a shift in the direction of trade winds decreases the intensity of the encounter with the terrestrial breeze, with lower contrast between the surface and the ocean temperatures. Another meteorological phenomenon contributing to the precipitation during this time of year is the ULCV, characterized as closed cyclone circulation with subsiding air in the center, and in these systems, the center has Clear Sky; however, its peripheries are submitted to large amounts of precipitation (Molion and Bernardo, 2002; Reboita *et al.*, 2012). The precipitation reaches 820.2 mm and 527.2 mm in the autumn and winter, respectively. In the rainy season (April to August) precipitation is caused due to the action of some weather systems dependent on the effect of some surface and atmosphere configurations. We can highlight the occurrence of the penetration of frontal systems that may in some cases reach equatorial latitudes (Kousky, 1979), the convergence of trade winds with the terrestrial breeze that reaches its peak during the autumn and winter seasons with the increasing contrast of temperature between earth and ocean (Kousky, 1980), the eastern undulating disturbances known as eastern waves (EW) (Chou, 1990; Espinoza, 1996), and finally the action of the South Atlantic Convergence Zone (SACZ) when moved to lower latitudes (near Equator). The SACZ configuration is related to the ITCZ positioning, causing good part of the precipitation in Maceió (Molion and Bernardo, 2000). The month of December has the longest sunshine duration (SD) (260.4 hours), followed by November (259.2 hours) (Fig. 3b). The months of June (164.7 hours) and July (165.4 hours) are those with the lowest SD.

In addition to its proximity to the Atlantic Ocean, Maceió is also influenced by the presence of two large lagoons: Mundaú and Manguaba. The Mundaú lagoon has an approximate reservoir of 23 km^2 and Manguaba with 42 km^2. Both are located within a radius of 15 km south of Maceió. Their dimensions represent a local microclimate, causing interference in the atmosphere and in the microphysics of clouds. With the convection of the ocean and

lagoons, the region of Maceió is strongly influenced by water vapor for most of the year (Fig. 4), helping in the formation and predominance of cumulus clouds in the local atmosphere. Water vapor accompanies the annual trend of air temperature and SD, increasing values in spring - summer and decreasing in autumn - winter.

3.2. Analysis of solar irradiance under clear sky conditions (CS)

Regardless of astronomical effect, on days whose sky has high atmospheric transmittance, the daytime solar irradiance variation is attributed only to atmospheric constituents (aerosols and water vapor, for example), mainly in the I_D magnitude (Gueymard, 2012). Aerosols can reach levels that attenuate I_D by approximately 70%, or more in extreme conditions (Ruiz-Arias *et al.*, 2016). Under CS, the daytime radiation components did not have large oscillations for DS, with total: $H_G^d = 27.52$ MJ m^{-2} and $H_D^d = 31.33$ MJ m^{-2}, morning values ($H_G = 16.34$ MJ m^{-2} and $H_D = 18.41$ MJ m^{-2}) and afternoon values ($H_G = 11.18$ MJ m^{-2} and $H_D = 12.92$ MJ m^{-2}) (Fig. 5a).
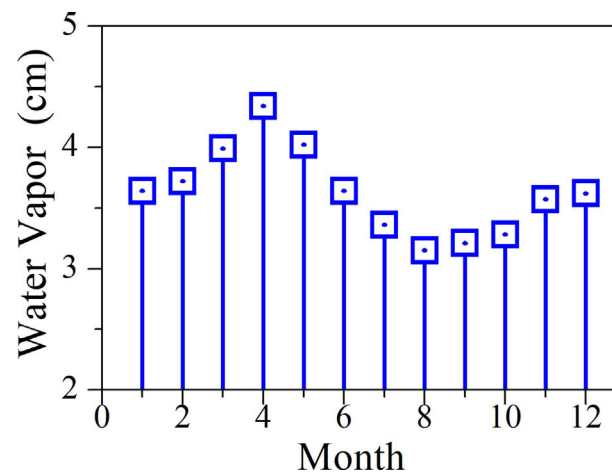
Figura 4 - Monthly average of water vapor in the atmosphere of Maceió. Source: Soda-pro.

H_D values in the morning (from sunrise to noon) and afternoon (from noon to sunset) are higher than H_G values for the same period. This can be caused by the atmospheric optical mass and the method of measuring the solar components that are different. While I_D (H_D) is measured directly (with the pyrheliometer) pointed at the solar disk (following diurnal solar trajectory), I_G (H_G) is measured with fixed sensor (pyranometer) on the horizontal surface. The daily average I_G and I_D were (687.2 ± 292.0 W m^{-2}) and (787.0 ± 148.6 W m^{-2}), respectively. The maximum I_G value is close to that observed in Maceió (Porfírio *et al.*, 2012) and higher than that found by Podstawczynska (2010). For six climatic zones in Nigeria and considering all types of sky cover condition, Chukwujindu and Julie (2017) found average values ranging from 6.30 to 28.8 MJm^{-2}.

In PRS, under CS conditions, daytime variation has a marked fluctuation caused by the passage of dispersed clouds in the atmosphere (Fig. 5b): with daily totals for $H_G{}^d = 26.99$ MJ m^{-2} and $H_D{}^d = 28.07$ MJ m^{-2}. Although it is characterized as clear sky day, the daily formation of transient clouds of the cumulus type is common at this time of year due to the proximity of the region to the

Atlantic Ocean, which in some cases may develop into other types of clouds, both of horizontal or vertical development. The maximum I_G and I_D values were 1107.0 W m^{-2} and 905.8 W m^{-2}, respectively. The daily average was $I_G = 672.1 \pm 329.5$ W m^{-2} and $I_D = 702.4 \pm 183.6$ W m^{-2}. During this period of year, negative variation may occur due to the decrease of the solar radiation available at the top of the atmosphere and the increase of the water vapor content in the atmosphere, which is absorbed with greater intensity. Similar values for I_G and I_D irradiance was found for different sites in Portugal (Cavaco *et al.*, 2016).

Also under CS conditions, for RS, the existence of greater oscillations and reduction of diurnal I_G and I_D values can be observed (Fig. 5c): with daily totals equal 20.90 MJ m^{-2} to H_G and 24.02 MJ m^{-2} to $H_D{}^d$ The maximum I_G and I_D values were 870.3 W m^{-2} and 824.0 W m^{-2}, with daily average of 529.8 ± 279.4 W m^{-2} and 632.0 ± 224.7 W m^{-2}, respectively. During this period, there is a decrease in the available solar radiation due to the greater solar declination in the Northern Hemisphere, increase in cloudiness and reduction in the water vapor content in the local atmosphere. In addition, it is also verified that
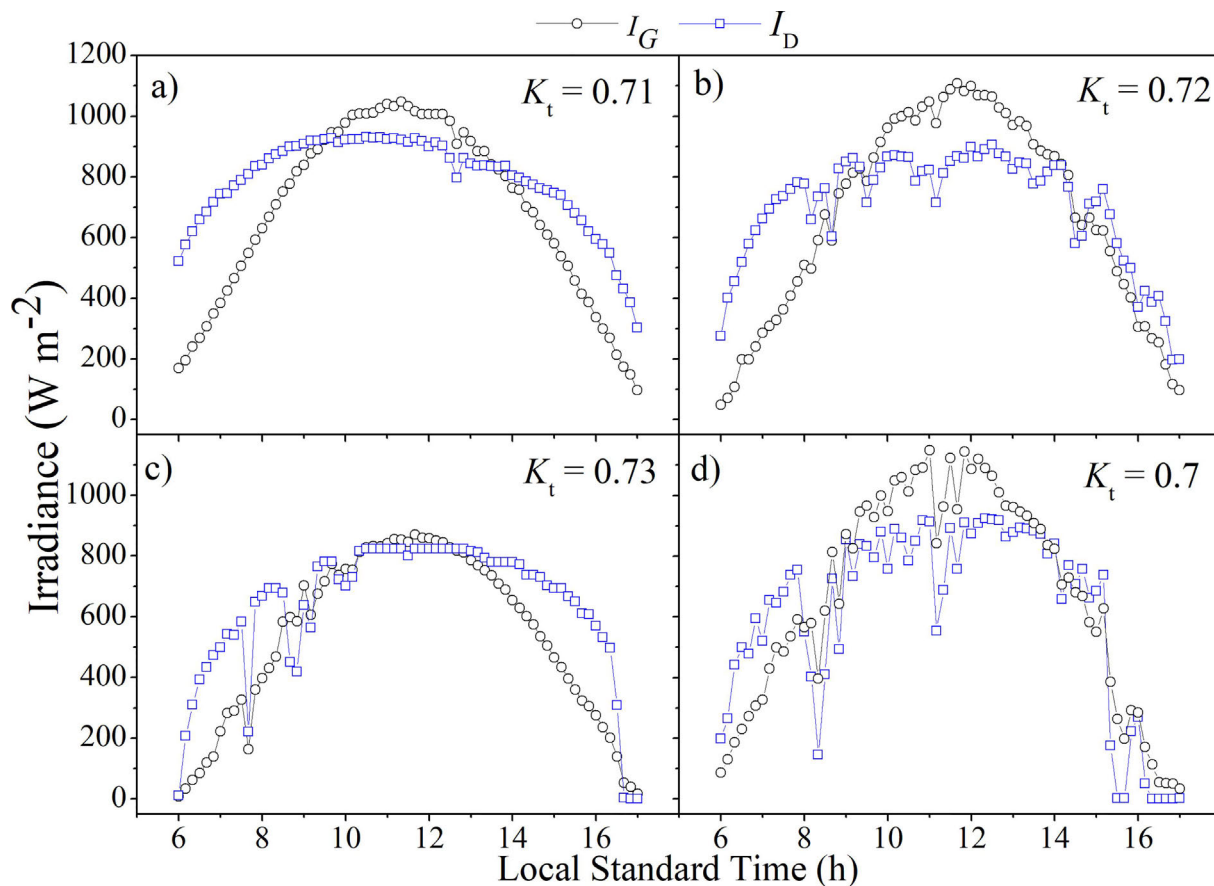
Figura 5 - Variation of global (I_G) and direct normal (I_D) solar irradiances under clear sky condition: (a) (12/12/2013) in dry season; (b) (03/17/2011) in pre-rainy season; (c) (06/24/2011) in rainy season; (d) (10/09/2012) in pre-dry season.

between 10:00 am and 01:00 pm, irradiance values are approximately constant, varying from (812.6 to 870.3 W m^{-2}) for I_G and from (815.2 to 816.3 W m^{-2}) for I_D.

Greater variations in values occurred in PDS during the daytime period, in which a sharp drop in the irradiance values was observed when I_G decreased from (627.3 to 385.1 W m^{-2}), and I_D from (738.6 to 175.4 W m^{-2}) (Fig. 5d). This oscillation is the result of the dynamics of cumulus clouds in the local atmosphere, because in this period (PDS), the water vapor in the atmosphere remains approximately constant. The maximum values observed for the day were I_G = 1149.1 W m^{-2} and I_D = 923.2 W m^{-2}, with daily totals H_G^d = 26.50 MJ m^{-2} and H_D^d = 24.52 MJ m^{-2}. It was observed that I_D increases with the elevation of I_G, revealing that I_D is controlled by the variation of I_G. Results similar to those from Maceió for I_D were obtained by Padova (northern Italy) and Trisaia (Southern Italy) (Dugaria *et al.*, 2015).

3.3. Analysis of solar irradiance under partially cloudy sky conditions (PCS)

Under PCS condition, the irradiance curves have larger fluctuations throughout the day, caused mainly by the dynamics of cumulus clouds in the atmosphere (Fig. 6a-d). The maximum peaks I_G and I_D values were higher under PCS condition than on CS days. This is explained by the

multi-reflections between the surface and the cloud bases, being phenomena typical of partially cloudy days, causing an increase of the descending reflection that increases the irradiance in comparison with cloud-free days (Porfirio *et al.*, 2012). Souza *et al.* (2005) in a study on the solar irradiance for Maceió observed the occurrence of multiple reflections, confirmed by I_G values very close to I_0. In different places in the State of Alagoas / Brazil, it has been reported that this phenomenon is not uncommon and occurs on at least one third of the days in a given month (Andrade and Tiba, 2016).

As expected, the H_G^d (20.52 MJ m^{-2}) and H_D^d values (18.19 MJ m^{-2}) under PCS condition for DS were lower than those obtained under CS condition (Fig. 6a). The maximum I_G and I_D values were 1123.0 W m^{-2} and 929.8 W m^{-2}, respectively, with average daily of I_G = 512.2 ± 292.6 W m^{-2} and I_D = 458.3 ± 314.3 W m^{-2}. The H_G^d values under these conditions were close to those observed by Porfirio *et al.* (2012). In the PRS, the irradiance that reached the surface was lower than in PDS, with daily average I_G and I_D values (maximum) of 507.6 ± 278.3 W m^{-2} (1099.6 W m^{-2}) and 306.4 ± 241.6 W m^{-2} (859.0 W m^{-2}), respectively (Fig. 6b). The irradiation values were 20.05 and 11.58 MJ m^{-2} for H_G^d and H_D^d, respectively. Similar values were observed by Polo *et al.* (2017).
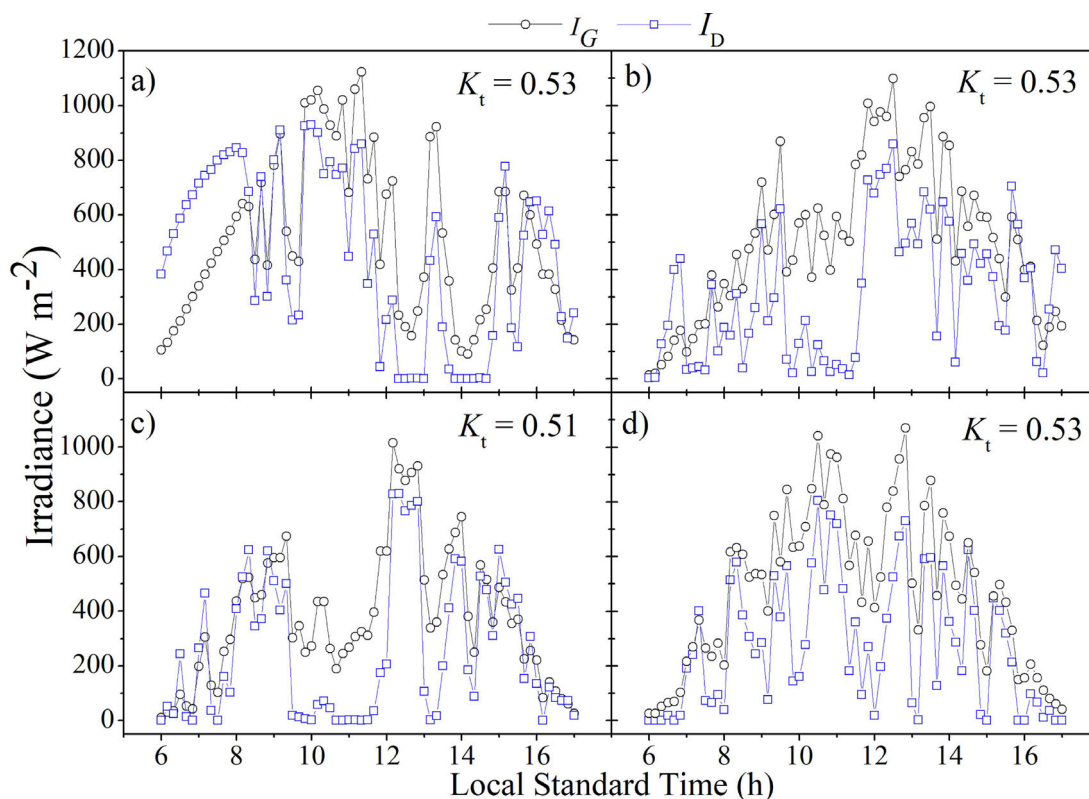
Figura 6 - Variation of global (I_G) and direct normal (I_D) solar irradiances under partially cloudy sky condition: (a) in dry season (01/09/2014), (b) in pre-rainy season (03/02/2013), (c) in rainy season (06/07/2012) and (d) in pre-dry season (09/17/2012).

The solar irradiance values in RS were smaller when compared to the other seasons, with a sharp decrease (between 09:00 am and 12:00 am) in I_G from (673.7 to 302.2 W m^{-2}), while I_D decreases from (500.7 to 18.8 W m^{-2}) (Fig. 6c). The irradiance remained low and increased to the maximum peak of I_G (1015.5 W m^{-2}) and I_D (827.5 W m^{-2}). The average daily irradiance values were I_G = 378.2 ± 244.5 W m^{-2} and I_D = 250.24 ± 257.60 W m^{-2}. During this period, cloudiness is the main responsible for the irradiance variations throughout the day. Irradiation values were 14.62 MJ m^{-2} and 9.49 MJ m^{-2} for $H_G{}^d$ and $H_D{}^d$, respectively. The average PRS values [I_G = 480.5 ± 288.0 W m^{-2} ($H_G{}^d$ = 19.29 MJ m^{-2}) and I_D = 272.2 ± 238.2 W m^{-2} ($H_D{}^d$ = 10.94 MJ m^{-2})] are higher than those observed in RS and smaller than those observed in PRS and DS (Fig. 6d). In four sites in Australia, Grantham *et al.* (2017) found diurnal curves for I_G and I_D under CS and OS conditions with the same behavior of results of this research. On day of OS, evidences of the transient effects of clouds causing fluctuations in I_D are observed. On day of CS, I_G and I_D do not exceed the value of 1000 W m^{-2}. In Maceió, values above this value are observed.

3.4. Analysis of solar irradiance under overcast sky conditions (OS)

Under OS condition, low I_G and I_D values are expected, since much of the solar irradiance cannot cross the Earth's atmosphere, being absorbed, reflected or scattered by clouds. In this condition, the clouds result in a reduction in I_D values. Therefore, the absence of clouds causes the elevation of I_G and I_D in CS days, while in OS days, I_D tends to zero and the I_G is significantly reduced to smaller values ($I_G \approx I_d$). Thus, under OS condition, the daily I_G values are greater than the daily I_D values. Studies have shown that I_D is much more sensitive than I_G for changes in the amounts of clouds and aerosols (Ruiz-Arias *et al.*, 2016). Moreover, in this sky cover, it is expected that the irradiance values for DS [I_G = 362.4 ± 161.3 W m^{-2} and I_D = 123.7 ± 188.2 W m^{-2}] are lower than those observed in the other conditions (Fig. 7a). Peak I_G and I_D values were 732.7 W m^{-2} and 625.3 W m^{-2}, respectively. It was observed that the morning, evening and daily H_G totals were one of the lowest values found, especially during the morning, whose I_D was almost non-existent, caused by cloud attenuation.
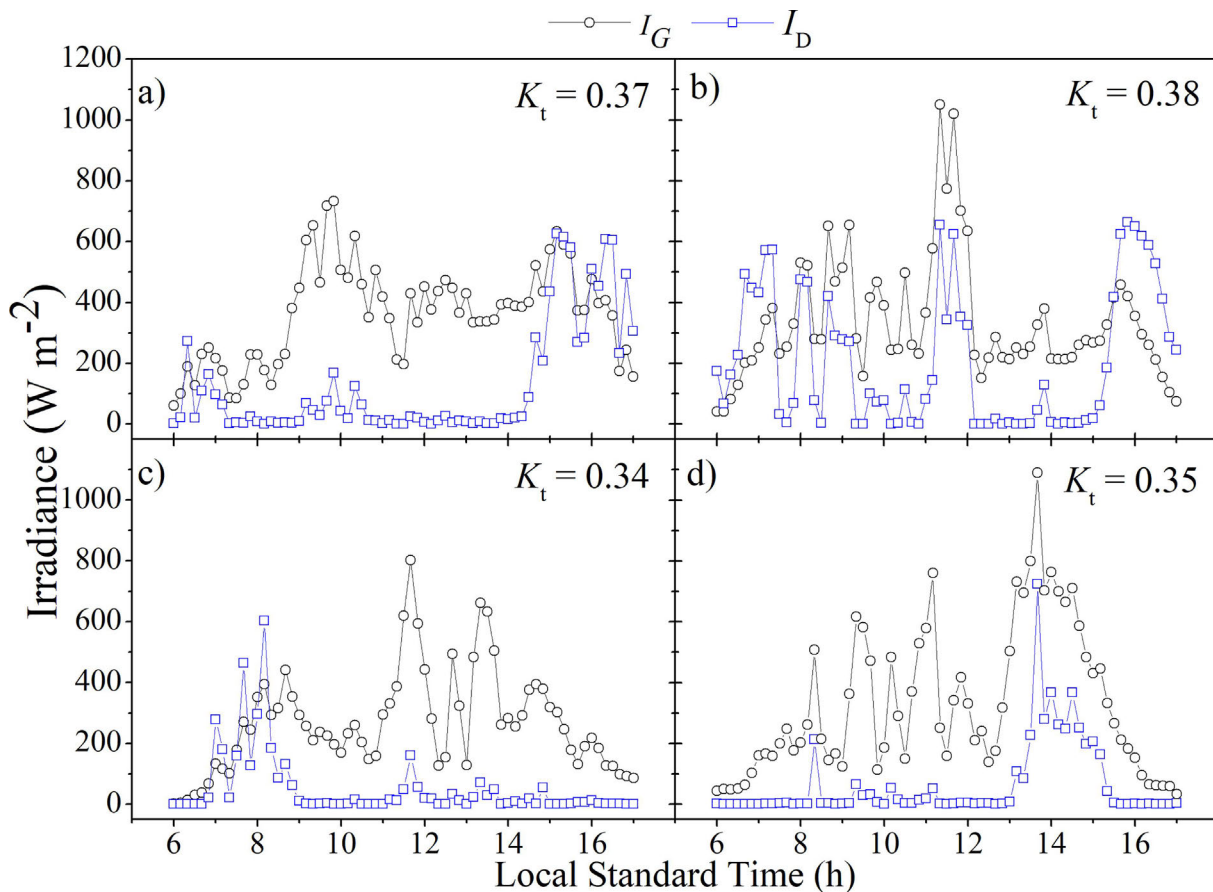
Figura 7 - Variation of global (I_G) and direct normal (I_D) solar irradiances under overcast sky condition: (a) (12/30/2012) in dry season, (b) (04/07/2014) in pre-rainy season, (c) (08/05/2013) in rainy season and (d) (10/01/2012) in pre-dry season.

In PRS, the average daily I_G and I_D values were equal to 335.5 ± 200.3 W m^{-2} and 208.3 ± 226.6 W m^{-2}, respectively (Fig. 7b). The daily H_G and H_D totals were equal to 13.46 and 8.24 MJ m^{-2}, respectively. In RS, I_D had values close to zero during the daytime period, the daily averages were $I_G = 265.0 \pm 166.6$ W m^{-2} ($H_G^d = 10.47$ MJ m^{-2}) and $I_D = 49.6 \pm 107.5$ W m^{-2} ($H_D^d = 1.94$ MJ m^{-2}), with daily maximum values of $I_G = 801.9$ W m^{-2} and $I_D = 603.0$ W m^{-2} (Fig. 7c). The daily totals were the lowest, since the selected day belongs to the rainy season and has low K_t value. In relation to OS days in RS (Souza *et al.*, 2005; Porifírio *et al.*, 2012) found similar values with measurements in the same location from different years. The average daily I_G and I_D values were 328.6 ± 243.3 W m^{-2} ($H_G^d = 13.18$ MJ m^{-2}) and 61.2 ± 126.3 W m^{-2} ($H_D^d = 2.38$ MJ m^{-2}) and daily peaks reached 1089.5 W m^{-2} and 723.7 W m^{-2}, respectively (Fig. 7d). Study I_G and I_D Souza *et al.* (2005), Vilani *et al.* (2006) and Porifírio *et al.* (2012) found values with the same quantitative characteristics regarding the periods of greatest and smallest oscillations. The influence of cloudiness on I_G and I_D levels is remarkable. In addition, atmospheric water vapor has strong absorption in the region of the infrared spectrum, being able to reduce significantly the values of irradiances incident on the surface. The small differences observed along the analyzed periods show that energy totals are more affected by cloudiness than by seasonal variation, when compared with days of CS.

3.5. Hourly average of the global ($\overline{I}_G^h$) and direct normal ($\overline{I}_D^h$) solar irradiance

In DS under CS condition, the maximum $\overline{I}_G^h$ value was 765.6 ± 100.0 W m^{-2} occurred between 09:00 am and 12:00 pm and was 728.2 ± 29.9 W m^{-2} (12:00 pm - 03:00 pm), which were the highest values found for CS (Table 1). Under PCS condition, the maximum $\overline{I}_G^h$ and $\overline{I}_D^h$

values were 608.6 ± 91.6 W m^{-2} and 420.5 ± 26.8 W m^{-2}, respectively. Under OS condition, $\overline{I}_G^h$ had maximum value of 354.9 ± 49.2 W m^{-2} and $\overline{I}_D^h$ with maximum value of 197.3 ± 16.7 W m^{-2}. The lowest values are found for OS condition and the highest values for the CS condition, evidencing the effect of clouds and atmospheric constituents on the attenuation of irradiances.

In PRS under CS condition, the maximum $\overline{I}_G^h$ and $\overline{I}_D^h$ values were 829.3 ± 105.0 W m^{-2} and 739.9 ± 31.8 W m^{-2}, which represents an increase of 8.31 and 1.59%, when compared to DS values (Table 2). For the PCS condition, the highest global and direct irradiance values were 674.2 ± 97.8 W m^{-2} and 425.2 ± 18.9 W m^{-2}, respectively, indicating an increase of 10.76% in $\overline{I}_G^h$ and 1.10% the $\overline{I}_D^h$ in relation to ES. Under OS condition, the maximum $\overline{I}_G^h$ and $\overline{I}_D^h$ values were 367.2 ± 40.2 W m^{-2} and 196.1 ± 3.6 W m^{-2}, respectively, an increase of 6.47% and decrease of 0.60% in comparison to DS. The lowest $\overline{I}_D^h$ values are observed in PRS under OS condition. As RS is prolonged, there is a relatively higher presence of clouds, increased humidity and absorption of near infrared (NIR) radiation of the solar spectrum, which produces low $\overline{I}_D^h$ magnitude.

Under CS condition for RS, irradiances had maximum $\overline{I}_G^h$ values = 712.2 ± 103.4 W m^{-2} and $\overline{I}_D^h$ values = 649.0 ± 37.7 W m^{-2}, reduction of $\approx 16.42\%$ and $\approx 14\%$ in relation to PRS, respectively (Table 3). Under PCS condition, the maximum $\overline{I}_G^h$ value was 572.6 ± 65.7 W m^{-2} (decrease of $\approx 17.73\%$) and $\overline{I}_D^h$ was 347.7 ± 10.5 W m^{-2} (reduction of $\approx 22.28\%$) compared to PRS. Under OS condition, $\overline{I}_G^h$ has maximum value of 354.0 ± 45.6 W m^{-2}, representing a reduction of $\approx 3.74\%$ when compared to PRS; $\overline{I}_D^h$ reached maximum value of 169.1 ± 59.7 W m^{-2}, with a decrease of $\approx 15.98\%$ compared to PRS.

Table 1 - Hourly average of the global ($\overline{I}_G^h$, W m^{-2}) and direct normal ($\overline{I}_D^h$, W m^{-2}) solar irradiances under different cloud cover for the dry season (November-February) with the respective standard deviations (δI_G^h and δI_D^h).

	06:00-09:00	09:00-12:00	12:00-15:00	15:00-17:00
	local time (h) interval			
	solar irradiance (W m^{-2}) under $K_t \geq 0.60$			
$\overline{I}_G^h \pm \delta I_G^h$	352.8 ± 143.1	765.6 ± 100.0	732.8 ± 125.7	305.1 ± 146.4
$\overline{I}_D^h \pm \delta I_D^h$	480.2 ± 48.5	644.2 ± 60.3	728.2 ± 29.9	469.4 ± 147.1
	solar irradiance (W m^{-2}) under $0.40 \leq K_t < 0.60$			
$\overline{I}_G^h \pm \delta I_G^h$	296.5 ± 145.8	608.6 ± 91.6	588.57 ± 86.7	244.06 ± 129.7
$\overline{I}_D^h \pm \delta I_D^h$	278.2 ± 34.73	354.2 ± 56.6	420.51 ± 26.8	301.08 ± 78.5
	solar irradiance (W m^{-2}) under $K_t < 0.40$			
$\overline{I}_G^h \pm \delta I_G^h$	164.0 ± 70.6	344.9 ± 49.2	316.28 ± 15.8	145.35 ± 72.3
$\overline{I}_D^h \pm \delta I_D^h$	197.3 ± 16.7	161.0 ± 17.7	159.44 ± 23.8	124.17 ± 32.6

The maximum $\overline{I}_G^h$ and $\overline{I}_D^h$ values under CS condition for PDS were 887.8 ± 103.7 W m^{-2} and 657.3 ± 46.7 W m^{-2}, respectively, increasing ≈ 24.64% and ≈ 1.27%

when compared to RS (Table 4). Under PCS conditions, the maximum $\overline{I}_G^h$ and $\overline{I}_D^h$ values were 690.9 ± 103.2 W m^{-2} and 406.9 ± 21.6 W m^{-2}, increase of 20.66% and

Table 2 - Hourly average of the global ($\overline{I}_G^h$, W m^{-2}) and direct normal ($\overline{I}_D^h$, W m^{-2}) solar irradiances under different cloud cover for the pre-rainy season (March and April) with the respective standard deviations (δI_G^h and δI_D^h).

	local time (h) interval			
	06:00-09:00	09:00-12:00	12:00-15:00	15:00-17:00
	solar irradiance (W m^{-2}) under $K_t \geq 0.60$			
$\overline{I}_G^h \pm \delta I_G^h$	336.0 ± 195.8	829.3 ± 105.0	796.8 ± 130.9	317.9 ± 164.9
$\overline{I}_D^h \pm \delta I_D^h$	407.1 ± 116.1	625.2 ± 83.5	739.9 ± 31.8	494.6 ± 131.3
	solar irradiance (W m^{-2}) under $0.40 \leq K_t < 0.60$			
$\overline{I}_G^h \pm \delta I_G^h$	279.9 ± 169. 6	674.2 ± 97.8	652.4 ± 110.4	253.6 ± 131.3
$\overline{I}_D^h \pm \delta I_D^h$	272.2 ± 60.1	365.4 ± 70.3	425.2 ± 18.9	311.4 ± 74.1
	solar irradiance (W m^{-2}) under $K_t < 0.40$			
$\overline{I}_G^h \pm \delta I_G^h$	191.5 ± 120.8	367.4 ± 40.2	338.3 ± 45.9	138.7 ± 77.2
$\overline{I}_D^h \pm \delta I_D^h$	101.6 ± 21.0	95.2 ± 23.6	41.4 ± 27.1	196.1 ± 3.6

Table 3 - Hourly average of the global ($\overline{I}_G^h$, W m^{-2}) and direct normal ($\overline{I}_D^h$, W m^{-2}) solar irradiances under different cloud cover for the rainy season (May-August) with the respective standard deviations (δI_G^h and δI_D^h).

	local time (h) interval			
	06:00-09:00	09:00-12:00	12:00-15:00	15:00-17:00
	solar irradiance (W m^{-2}) under $K_t \geq 0.60$			
$\overline{I}_G^h \pm \delta I_G^h$	285.5 ± 195.7	712.2 ± 103.4	666.5 ± 113.5	252.6 ± 146.9
$\overline{I}_D^h \pm \delta I_D^h$	423.3 ± 181.4	583.5 ± 91.7	649.0 ± 37.7	405.1 ± 132.5
	solar irradiance (W m^{-2}) under $0.40 \leq K_t < 0.60$			
$\overline{I}_G^h \pm \delta I_G^h$	228.5 ± 159.0	572.6 ± 65.7	532.0 ± 91.6	187.4 ± 112.0
$\overline{I}_D^h \pm \delta I_D^h$	247.0 ± 88.0	321.9 ± 20.7	347.7 ± 10.5	227.5 ± 54.5
	solar irradiance (W m^{-2}) under $K_t < 0.40$			
$\overline{I}_G^h \pm \delta I_G^h$	149.0 ± 101.9	354.0 ± 45.6	332.8 ± 62.1	114.3 ± 71.5
$\overline{I}_D^h \pm \delta I_D^h$	169.1 ± 59.7	113.7 ± 16.5	117.0 ± 8.7	103.2 ± 67.7

Table 4 - Hourly average of the global ($\overline{I}_G^h$, W m^{-2}) and direct normal ($\overline{I}_D^h$, W m^{-2}) solar irradiances under different cloud cover for the pre-dry season (September and October) with the respective standard deviations (δI_G^h and δI_D^h).

	Local time (h) interval			
	06:00-09:00	09:00-12:00	12:00-15:00	15:00-17:00
	solar irradiance (W m^{-2}) under $K_t \geq 0.60$			
$\overline{I}_G^h \pm \delta I_G^h$	373.5 ± 177.8	887.8 ± 103.7	803.5 ± 156.4	279.3 ± 180.5
$\overline{I}_D^h \pm \delta I_D^h$	370.2 ± 101.1	586.4 ± 29.8	657.3 ± 46.7	360.3 ± 169.9
	solar irradiance (W m^{-2}) under $0.40 \leq K_t < 0.60$			
$\overline{I}_G^h \pm \delta I_G^h$	310.0 ± 153. 8	690.9 ± 103.2	624.7 ± 94.5	226.7 ± 136.7
$\overline{I}_D^h \pm \delta I_D^h$	215.8 ± 36.6	372.0 ± 61.0	406.9 ± 21.6	278.7 ± 132.1
	solar irradiance (W m^{-2}) under $K_t < 0.40$			
$\overline{I}_G^h \pm \delta I_G^h$	216.53 ± 107.48	414.18± 8.24	442.92± 70.28	163.8 ± 103.1
$\overline{I}_D^h \pm \delta I_D^h$	298.24 ± 68.55	394.40 ± 114.82	532.03± 35.76	381.4 ± 97.6

17.01% with respect to RS. Under OS condition, he maximum $\overline{I}_G^h$ and $\overline{I}_D^h$ values were 442.9 $\pm$ 70.2 W m^{-2} and 532.0 $\pm$ 35.8 W m^{-2}, increase of $\approx$ 25.12% for $\overline{I}_G^h$ and $\approx$ 314.66% for $\overline{I}_D^h$.

3.6. Hourly solar irradiation

Figure 8 shows the average hourly global solar irradiation ($\overline{H}_G^h$) observed for all four seasons (obtained through the average irradiation of each hour interval). The diurnal variation among the different seasons is the same, increasing from morning until reaching maximum near noon and then falling until the end of the afternoon. In relation to this behavior, the hourly values tend to spread symmetrically to the solar half day. The largest curve amplitude is in DS, followed by PDS, PRS and RS. This behavior evidences the solar declination effect among seasons, the amplitude decreases as the day of the year distances from the summer solstice. The diurnal evolution is characterized by the effect of the zenith angle, since $\overline{H}_G^h$ is measured in the horizontal plane. In DS, the total H_G value in the day is 22.47 MJ m^{-2}, and the morning and afternoon values were 12.01 and 10.47 MJ m^{-2}, respectively. The diurnal evolution in PRS has a decrease in values when compared to DS, H_G^d was 20.45 MJ m^{-2}, with maximum hourly value ($\overline{H}_G^h$ = 2.90 MJ m^{-2}). In RS, the hourly averages and the daily total (H_G^d = 15.45 MJ m^{-2}) had the greatest reduction, and the maximum value at this season was $\overline{H}_G^h$ = 2.24 MJ m^{-2}. The diurnal evolution in PDS for H_G^d = 20.45 MJ m^{-2} and maximum hourly $\overline{H}_G^h$ = 2.91 MJ m^{-2}. Approximate $\overline{H}_G^h$ values were also found by researchers Souza *et al*. (2005), Marques Filho *et al*. (2016) and Tahir and Asim (2018). Although they are not located at the same latitude, the results of Maceió are similar to those obtained at sites in Nigeria by Osinowo *et al*. (2015), which found a uniform pattern in the distribution of $\overline{H}_G^h$

values, with peaks ranging from (15.01 to 12.01) MJ m^{-2} and with results observed in Saudi Arabia (AlYahya and Irfan, 2016).

The daytime variation of $\overline{H}_G^h$ has a decrease after 08:00 am returning to increase soon after. This is due to the greater cloudiness in the morning, caused by the effect of local wind circulation (sea breezes), which are responsible for creating a zone of convergence near the coast (front breeze), contributing to the formation of cumulus clouds until near 01:00 pm, when it is verified the formation of an area of suppression of cumulus clouds related to the displacement of the zones of breeze subsidence and convergence (National Research Council, 1992; Silva, 2003). This effect is more intense in H_D because this component is measured with the sensor directly pointed at the solar disk. In DS, H_D has value of 17.20 MJ m^{-2} and maximum hourly average direct solar normal ($\overline{H}_D^h$) value = 2.00 MJ m^{-2} (Fig. 8b). In PRS, the H_D values were higher than in DS, with H_D = 18.38 MJ m^{-2} and maximum $\overline{H}_D^h$ = 2.23 MJ m^{-2}. $\overline{H}_D^h$ has the lowest values in RS, with = 12.48 MJ m^{-2} and maximum peak $\overline{H}_D^h$ = 1.46 MJ m^{-2}. In PDS, H_D was 14.88 MJ m^{-2} and maximum $\overline{H}_D^h$ = 1.90 MJ m^{-2}. The seasonal variation in the $\overline{H}_D^h$ transmission is associated with sky cover conditions: large (small) K_t values are related to large (small) values of the $\overline{H}_D^h$ transmission. The local results resemble those obtained for two sites in Cyprus by Pashiardis *et al*. (2017), who performed a statistical analysis of H_D values, results found by Marques Filho *et al*. (2016) for Rio de Janeiro and for locations in Kenya (Kariuki and Sato, 2018), with values from satellite and two places of Morocco (Gairaa *et al*., 2017).

3.7. Frequency distribution of daily direct normal solar irradiance (I_D^d) in the different sky cover conditions

In the frequency distribution of I_D^d for CS condition in the four seasons, it was observed that the I_D^d values in
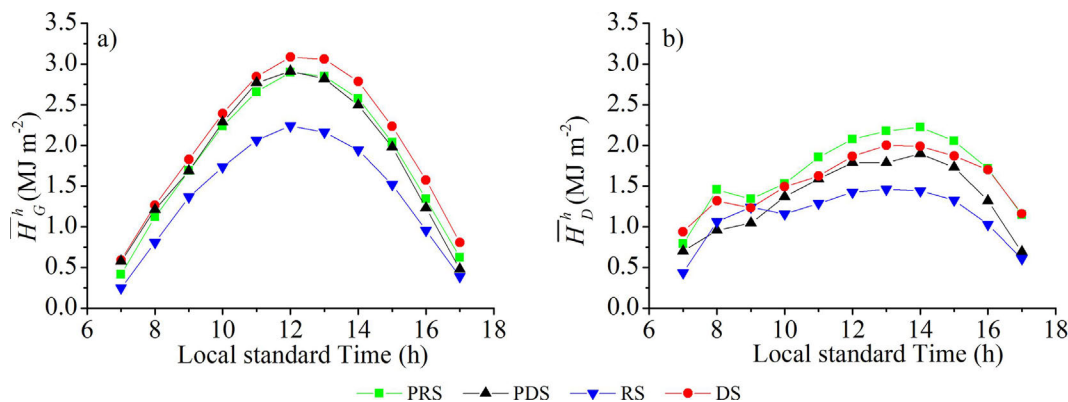
Figura 8 - The hourly average solar irradiation: a) global ($\overline{H}_G^h$); b) direct solar normal ($\overline{H}_D^h$). dry season (DS), pre-rainy season (PRS), rainy season (RS) and pre-dry season (PDS).

DS had greater occurrence between 400 and 600 W m^{-2}, comprising a relative occurrence rate of 68.8% of days, with higher occurrence of I_D^d for 440 W m^{-2} (Fig. 9a). Between 160 and 400 W m^{-2}, I_D^d maintained at a relative occurrence rate of 13.6% and from 600 W m^{-2} up to the maximum value (740 W m^{-2}), the relative occurrence rate corresponded to 17.6%. I_D^d in PRS had relative occurrence rate of 65.91% between 400 and 600 W m^{-2}, between 257.5 and 400 W m^{-2}, the occurrence of I_D^d remained with relative occurrence rate of 15.69%, but from 600 to 700 W m^{-2}, the relative occurrence rate corresponded 18.19% of days (Fig. 9b). For RS, I_D^d had higher relative occurrence rate between 400 and 600 W m^{-2}, which corresponds to about 60.92% of days of this season and from 252.5 to 400 W m^{-2}, the occurrence reached 39.08% of cases (Fig. 9c). In PDS, I_D^d values between 385 and 635 W m^{-2} corresponded to half the relative occurrence rate of all values, the other half was between 235 and 385 W m^{-2} and the interval with the highest relative occurrence rate was between 385 and 435 W m $^{-2}$, which totaled 27.77% (Fig. 9d). For the city of Daejeon, in South Korea, Lee *et al.* (2017) showed higher relative occurrence rate for 50 W m^{-2}, followed by 850 W m^{-2} and with lower relative occurrence rate for 950 W m^{-2}.

Under PCS condition, I_D^d for DS showed higher occurrence between 250 and 450 W m^{-2}, totaling a relative occurrence rate of 55.43%, from 10 to 250 W m^{-2}, the relative occurrence rate was 41.30%, in the interval from 450 W m^{-2} up to the maximum value (I_D^d = 590 W m^{-2}), the relative occurrence rate was 3.27% (Fig. 10a). In PRS, I_D^d had relative occurrence rate of 60.47% for the interval from 200 to 400 W m^{-2} (Fig. 10b). From 60 to 200 W m^{-2}, the percentage of I_D^d was 19.76% and from 400 to 600 W m^{-2}, corresponding to relative occurrence rate of 19.77%. The highest occurrence value of I_D^d was for the 300 W m^{-2}. In the relative occurrence rate histograms of I_D^d for RS (Fig. 10c), higher occurrence was observed close to 230 W m^{-2}, with higher relative occurrence rate (80%) between 38 and 308 W m^{-2}. In PDS, most occurrences of I_D^d were between 25 and 275 W m^{-2}, totaling a relative occurrence rate of 70.83%, between 275 and 675 W m^{-2} the relative occurrence rate of was 29.17% (Fig. 10d). In Seville - Spain, Moreno-Tejera *et al.* (2016) found that 42.4% of I_D values F are higher than 600 W m^{-2}, with higher relative occurrence rate of high values close to the summer solstice of the Southern Hemisphere.

Under OS condition, the behavior of I_D^d is different from the other sky covers, since the higher relative occurrence rate for values smaller than 100 W m^{-2} as observed
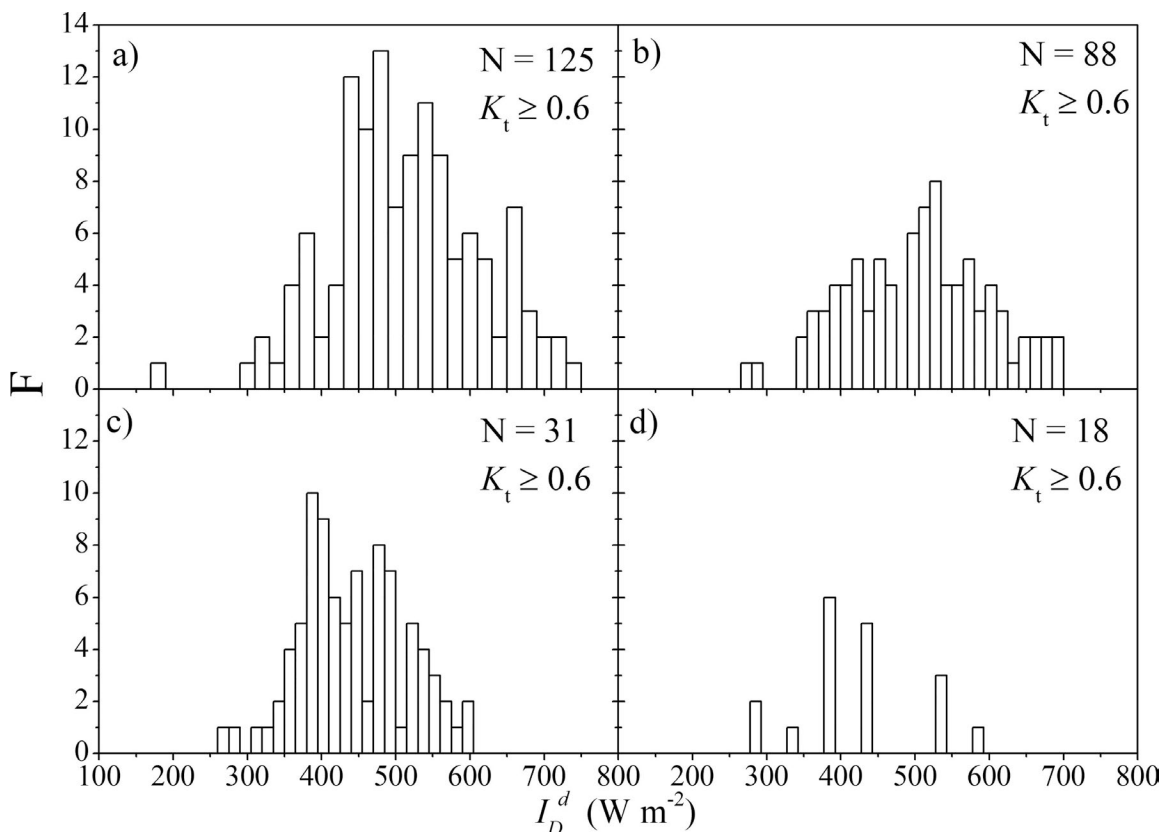
Figura 9 - Frequency distribution (F) of daily direct normal solar irradiance (I_D^d) under clear sky conditions: a) dry season; b) pre-rainy season; c) rainy season and d) pre-dry season. N = number of days.
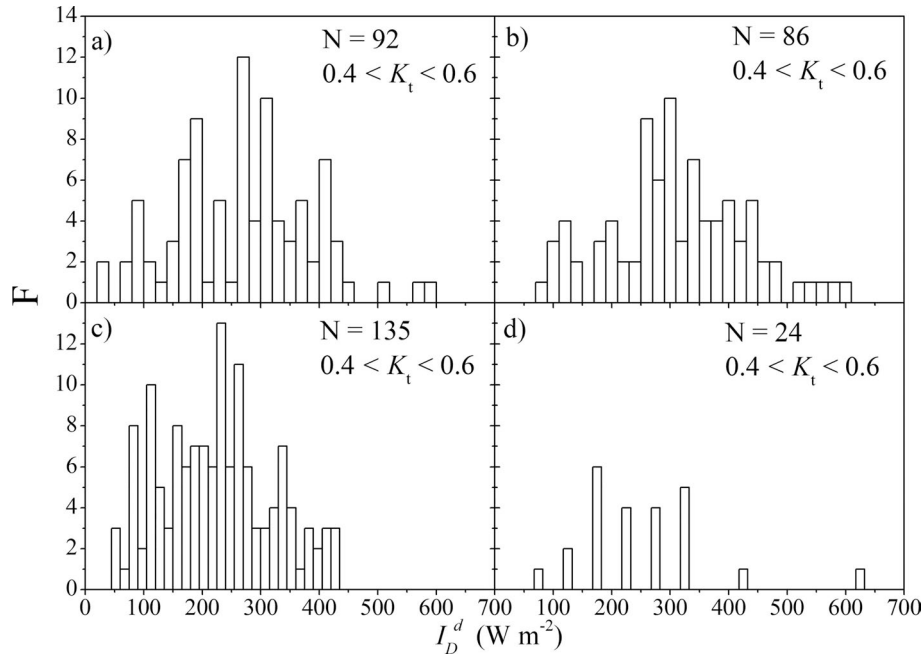
Figura 10 - Frequency distribution (F) of daily direct normal solar irradiance ($I_D{}^d$) under partially cloudy sky conditions: a) dry season; b) pre-rainy season; c) rainy season and d) pre-dry season. N = number of days.

in DS (Fig. 11a), whose greatest occurrences were up to 188 W m^{-2}, corresponding to a relative occurrence rate of 71.42% and in the interval from 188 to 563 W m^{-2}, the corresponding relative occurrence rate is 28.58%. For PRS, all $I_D{}^d$ measurements were not higher than 200 W m^{-2}, with 55% of the relative occurrence rate up to 100 W m^{-2} (Fig. 11b). In RS, the maximum value was 155 W m^{-2}, and up to 105 W m^{-2}, the relative occurrence rate was 80.64% and from 105 to 155 W m^{-2}, the relative occurrence rate was 19.36% (Fig. 11c). In PDS, the $I_D{}^d$
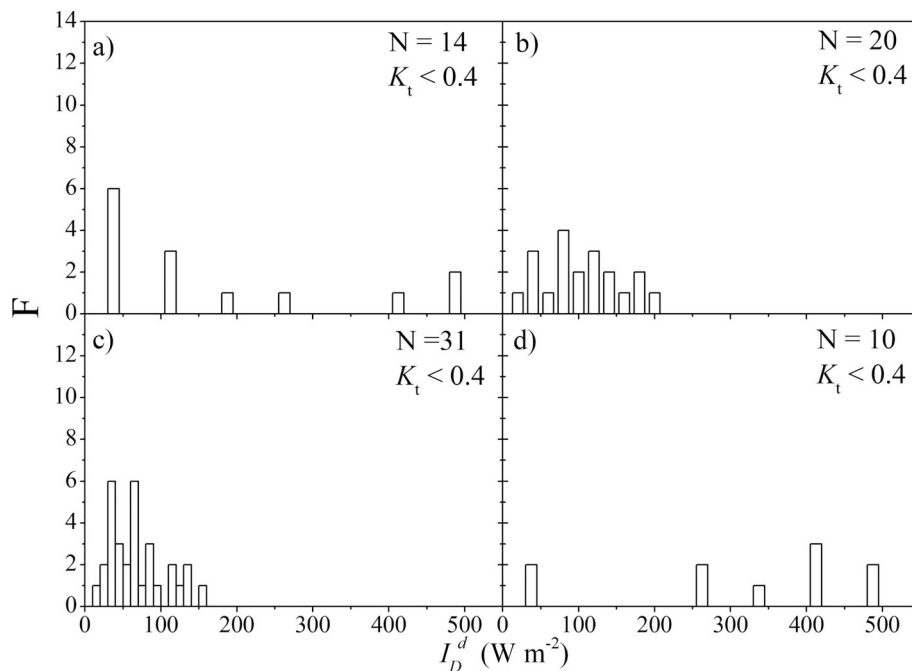
Figura 11 - frequency distribution (F) of daily direct normal solar irradiance ($I_D{}^d$) under overcast sky conditions ($K_t < 0.40$): a) dry season; b) pre-rainy season; c) rainy season and d) pre-dry season. N = number of days.

values increased and the accumulated relative occurrence rate reached 100% up to a maximum of 488 W m^{-2} and 50% up to 338 W m^{-2} (Fig. 11d).

4. Final considerations

Cumulus clouds were mainly responsible for seasonal oscillation and irradiance attenuation, significantly reducing surface values. It was observed the phenomenon of multireflections that resulted in peaks and maximum values in the condition of partly cloudy days.

The instantaneous global and direct normal solar irradiance for seasonal periods showed maximum values close to noon, especially for clear sky conditions (global atmospheric transmittance, $K_t \geq 0.60$).

Higher oscillations were found in the intermediate seasonal periods (pre-rainy season - PRS and pre-dry season - PDS).

The daily totals of global and direct normal solar irradiation have greater variations due to the cloudiness than astronomical factors (seasonality), being the greatest values found, in the majority, in the morning during the dry and pre-rainy season.

The average daily totals of the global hourly solar irradiation were higher during the dry season, different from the direct totals that were higher in the pre-rainy season.

The lowest cloudiness levels were observed in the dry season, followed by pre-rainy, pre-dry and rainy seasons.

The relative occurrence rate of direct normal irradiance in the daily partition under conditions of $K_t \geq 0.60$ was greater between 400 and 700 W m^{-2}. Under conditions of $0.4 \leq K_t < 0.6$, I_D^d occurred more between 200 and 500 W m^{-2} and under conditions of $K_t < 0.4$, it was below 200 W m^{-2}.

Therefore, according to the obtained results, it could be inferred that the patterns of solar incidence in the region of study are dependent on the cloudiness conditions. On the other hand, seasonality is a secondary factor that has little influence on the configuration of energy patterns. Thus, it was possible to characterize the distribution of direct normal solar irradiance for the region of Maceió, but there is still a need to intensify these studies for better understanding and application in several human activities, notably engineering, energy, agriculture, health and environment.

Acknowledgments

References

AlYahya, S.; Irfan, M.A. Analysis from the new solar radiation Atlas for Saudi Arabia. **Solar Energy**, v. 130, p. 116-127, 2016.

Andrade, R.C.; Tiba, C. Extreme global solar irradiance due to cloud enhancement in northeastern Brazil. **Renewable Energy**, v. 86, p. 1433-1441, 2016.

Barros, A.H.C.; Araujo Filho, J.C.; Silva, A.B.; Santiago, G.A.C.F. **Climatologia do Estado de Alagoas**. Recife: EMBRAPA SOLOS, 32p., 2012.

Cavaco, A.; Canhoto, P.; Costa, M.J.; Collares-Pereira, M. DNI measurements in the South of Portugal: Long term results through direct comparison with global and diffuse radiation measurements and existing time series. **AIP Conference Proceedings** 1734, 150001, 2016.

Chou, S.C. **Análise de Distúrbios Ondulatórios de Leste Sobre o Oceano Atlântico Equatorial Sul**. Dissertação de Mestrado em Meteorologia, Instituto Nacional de Pesquisas Espaciais, São José dos Campos, 134 p., 1990.

Chukwujindu, N.S.; Julie, O. Estimation of direct normal irradiance under various sky conditions in data sparse tropical ecological zones in Nigeria. **Internacional Journal of Advanced Astronomy**, v. 5, n. 2, p. 90-105, 2017.

Codato, G.; Oliveira, A.P.; Soares, J.; Escobedo, J.F.; Gomes, E.N.; Pai, A.D. D. Global and diffuse solar irradiances in urban and rural areas in southeast Brazil, **Theor. Appl. Climatol.**, v. 93, p. 57-73, 2008.

Dugaria, S.; Padovan, A.; Sabatelli, V.; Del Col, D. Assessment of estimation methods of DNI resource in solar concentrating systems. **Solar Energy**, v. 121, p. 103-115, 2015.

Espinoza, E.S. **Distúrbios nos Ventos de Leste no Atlântico Tropical**. São José dos Campos: INPE, 149p., 1996.

Evseev, E.G.; Kudish, A.I. Analysis of solar irradiation measurements at Beer Sheva, Israel from 1985 through 2013. **Energy Conversion and Management**, v. 97, p. 307-314, 2015.

Ferreira Junior, R.A.; Souza, J.L.; Lyra, G.B.; Escobedo, J.F.; Santos, M.V.C. C. Energy conversion efficiency in sugarcane under two row spacings in northeast of Brazil. **Revista Brasileira de Engenharia Agrícola e Ambiental**, v. 19, n. 8, p. 741-747, 2015.

Gairaa, K.; Khellaf, A.; Benkacilai, S.; Guermoui, M. Solar radiation measurements in Algeria: case of Ghardaïa station as member of the enerMENA meteorological network. **Energy Procedia**, v. 141, p. 50-54, 2017.

Grantham, A.P; Pudney, P.J.; Ward, L.A.; Belusko, M.; Boland, J.W. Generating synthetic five-minute solar irradiance values from hourly observations. **Solar Energy**, v. 147, p. 209-221, 2017.

Gueymard, C.A. Temporal variability in direct and global irradiance at various time scales as affected by aerosols. **Solar Energy**, v. 86, p. 3544-3553, 2012.

Iqbal, M. **An Introduction to Solar Radiation**. New York: Academic Press, 390 p., 1983.

Kariuki, B.W.; Sato, T. Interannual and spatial variability of solar radiation energy potential in Kenya using Meteosat satellite. **Renewable Energy**, v. 116, Parte A, p. 88-96, 2018.

Kaskaoutis, D.G.; Kambezidis, H.D. The diffuse-to-global and diffuse-to-direct-beam spectral irradiance ratios as turbidity

indexes in an urban environment. **Journal of Atmospheric and Solar-Terrestrial Physics**, v. 71, n. 2, p. 246-256, 2009.

Kotti, M.C.; Argiriou, A.A.; Kazantzidis, A. Estimation of direct normal irradiance from measured global and corrected diffuse horizontal irradiance. **Energy**, v. 70, n. 1, p. 382-392, 2014.

Kousky, V.E. Diurnal raifall variation on Northeast Brazil. **Monthly Weather Review**, v. 108, n. 4, p. 488-498, 1980.

Kousky, V.E. Frontal influences on Northeast Brazil. **Monthly Weather Review**, v. 107, n. 9, p. 1140-1153, 1979.

Lee, H-J.; Kim, S-Y.; Yun, C-Y. Comparison of Solar Radiation Models to Estimate Direct Normal Irradiance for Korea. **Energies**, v. 10, n. 5, p. 594, 2017.

Lima, M.C. **Variabilidade da Precipitação no Litoral Leste da Região Nordeste do Brasil**. Dissertação de Mestrado em Meteorologia, INPE - 5283 - TDI/453, 1991.

Liou, K.N. An Introduction to Atmospheric Radiation. 2. Ed. San Diego: Academic Press, 2002, 583p.

Liu, B.Y.H.; Jordan, R.C. The interrelationship and characteristic distribution of direct, diffuse and total solar radiation. **Solar Energy**, v. 4, n. 3, p. 1-19, 1960.

Lyra, G.B.; Oliveira Júnior, J.F.; Zeri, M. Cluster analysis applied to the spatial and temporal variability of monthly rainfall in Alagoas state, Northeast of Brazil. **Internat Journ Climat**, v. 34, n. 13, p. 3546-3558, 2014.

Marques Filho, E.P.; Oliveira, A.P.; Vita, W.A. et al. Global, diffuse and direct solar radiation at the surface in the city of Rio de Janeiro: Observational characterization and empirical modeling. **Renewable Energy**, v. 91, p. 64-74, 2016.

Molion, L.C.B.; Bernardo, S.O. Dinâmica das chuvas sobre o Nordeste do Brasil. In: **Congresso Brasileiro de Meteorologia**, 11, Rio de Janeiro, p. 1334-1342, 2000.

Molion, L.C.B.; Bernardo, S.O. Uma revisão da dinâmica das chuvas no nordeste brasileiro. **Revista Brasileira de Meteorologia**, v. 17, n. 1, p. 1-10, 2002.

Moreno-Tejera, S.; Silva-Perez, M.A.; Lillo-Bravo, I.; Ramırez-Santigosa, L. L. Solar resource assessment in Seville, Spain. Statistical characterisation of solar radiation at different time resolutions. **Solar Energy**, v. 132, p. 430-441, 2016.

Muneer, T. **Solar Irradiation and Daylight Models**. 2nd ed. Amsterdam: Elsevier, 2004.

National Research Council. 1992. Coastal Meteorology: A Review of the State of the Science. Washington: The National Academy Press, 1992. 112 p.

Oliveira, A.P.; Machado, J. A.; Escobedo, J. F.; Soares, J. Diurnal evolution of solar irradiation at the surface in the city of Sao Paulo: Seasonal variation and modeling, **Theor. Appl. Climatol.**, v. 71, n. 3-4, p. 231-249, 2002.

Osinowo, A.A.; Okogbue, E.C.; Ogungbenro, S.B.; Fashanu, O. Analysis of Global Solar Irradiance over Climatic Zones in Nigeria for Solar Energy Applications. Journal of Solar Energy, Volume 2015, Article ID 819307, 9 p.

Pashiardis, S.; Kalogirou, S.A.; Pelengaris, A. Statistical analysis for the characterization of solar energy utilization and intercomparison of solar radiation at two sites in Cyprus. **Applied Energy**, v. 190, p. 1138-1158, 2017.

Podstawczynska, A. UV and global solar radiation in Lodz, central Poland. **International Journal Climatology**, v. 30, n. 1, p. 1-10, 2010.

Polo, J.; Fernández-Peruchena, C.; Gastón, M. Analysis on the long-term relationship between DNI and CSP yield production for different technologies. **Solar Energy**, v. 155, p. 1121-1129, 2017.

Porfîrio, A.C.S.; Souza, J.L.; Lyra, G.B.; Lemes, M.A.M. An assessment of the global UV solar radiation under various sky conditions in Maceió-Northeastern Brazil. **Energy**, v. 4 4, n. 1, p. 584-592, 2012.

Reboita, M.S.; Krusche, N.; Ambrizzi, T.; Porfîrio, R. Entendendo o tempo e o clima na América do Sul. **Terrae Didatica**, v. 8, n. 1, p.34-50, 2012.

Ruiz-Arias, J.A.; Gueymard, C.A.; Santos-Alamillos, F.J.; Pozo-Vázquez, D. D. Worldwide impact of aerosol's time scale on the predicted long-term concentrating solar power potential. **Scientific Reports**, 6, 30546, 2016.

Santos, C.M.; Escobedo, J.F.; Teramoto, E.T.; Silva, S.H.M.G. Assessment of ANN and SVM models for estimating normal direct irradiation (H_b). **Energy Conversion and Management**, v. 126, p. 826-836, 2016.

Santos, C.M.; Souza, J.L.; Ferreira Junior, R.A.; Tiba, C.; Melo, R.O. *et al.* On modeling global solar irradiation using air temperature for Alagoas State, Northeastern Brazil. **Energy**, v. 71, p. 388-398, 2014.

Silva, G.R. **Características de Vento na Região Nordeste: Análise, Modelagem, e Aplicações Para Projetos de Centrais Eólicas**. Dissertação de Mestrado em Engenharia Mecânica, Universidade Federal de Pernambuco, Recife, 141 p., 2003.

Souza, J.L.; Moura Filho, G.; Fonseca, R.F.; Teodoro, I.; Santos, E.A. *et al.* Análise da precipitação pluvial e temperatura do ar na região do Tabuleiro Costeiro de Maceió, AL, período 1972 - 2001. **Revista Brasileira de Agrometeorologia**, v. 11, n. 2, p.131-141, 2004.

Souza, J.L.; Lima, F.Z. **Clima - Estudo de Impactos Ambiental, Levantamento Ambiental e Relatório, no Meio Ambiente de Área de Proteção Ambiental de Piaçabuçu - AL**. In: Relatório Técnico, Maceió: UFAL, p. 180-238, 1995.

Souza, J.L.; Nicácio, R.M.; Moura, M.A.L. Global solar radiation measurements in Maceió, Brazil. **Renewable Energy**, v. 30, n. 8, p. 1203-1220, 2005.

Tabari, H.; Talaee, P.H. Sensitivity of evapotranspiration to climatic change in different climates. **Glob. Planet. Chang**., v. 115, p. 16-23, 2014.

Tahir, Z.R.; Asim, M. Surface measured solar radiation data and solar energy resource assessment of Pakistan: A review. **Renewable and Sustainable Energy Reviews**, v. 81, Parte 2, p. 2839-2861, 2018.

Tiba, C. Solar radiation in the Brazilian Northeast. **Renewable Energy**, v. 22, p. 565-578, 2001.

Vick, B.D.; Daryl, R.; Myers, D.R.; Boyson, W.E. Using direct normal irradiance models and utility electrical loading to assess benefit of a concentrating solar power plant. **Solar Energy**, v. 86, n. 12, p. 3519-3530, 2012.

Vilani, M.T.; Sanches, L.; Nogueiram, J.S.; Priante Filho, N. Sazonalidade da radiação, temperatura, e umidade em uma

floresta de transição Amazônia Cerrado. **Revista Brasileira de Meteorologia**.v. 21, n. 3b, p. 331-343, 2006.

WMO. **Guide to Meteorological Instruments and Methods of Observation**. WMO-n°8, Seventh Edition, 157-197, Geneva, Switzerland, 2008.

Internet Resources

http://www.soda-pro.com/home

Nomenclature

I_G: global solar irradiance, W m^{-2}

I_D: direct normal solar irradiance, W m^{-2}

I_d: diffuse solar irradiance, W m^{-2}

I_0: irradiance at the top of the atmosphere, W m^{-2}

H_G: global solar irradiation, MJ m^{-2}

H_D: direct normal solar irradiation, MJ m^{-2}

H_0: irradiation at the top of the atmosphere, MJ m^{-2}

K_t: clearness index, adimensional

$\overline{I}_G^h$: average hourly of global solar irradiance, W m^{-2}

δI_G^h: standard deviations of $I_G{}^h$, W m^{-2}

$\overline{I}_D^h$: average hourly of direct normal solar irradiance, W m^{-2}

δI_D^h: standard deviations of $\overline{I}_D^h$, W m^{-2}

I_{SC} : solar constant, 1367 W m^{-2}

E_0: correction factor of the eccentricity of the Earth's orbit

θ_z: zenith angle

NEB: Northeastern Brazil

ITCZ: Intertropical Convergence Zone

ULCV: Upper-Level Cyclonic Vortexes

EW: Eastern Waves

SACZ: South Atlantic Convergence Zone

SD: sunshine duration

DS: Dry Season

PRS: Pre-Rainy Season

RS: Rainy Season

PDS: Pre-Dry Season

CS: Clear Sky

PCS: Partially Cloudy Sky

OS: Overcast Sky

Upper index

h: Hourly

d: Daily